A&A 673, L5 (2023)
https://doi.org/10.1051/0004-6361/202345875

Astronomy & Astrophysics
Special issue

Solar Orbiter First Results (Nominal Mission Phase)

LETTER TO THE EDITOR

Recurrent ^{3}He-rich solar energetic particle injections observed by Solar Orbiter at ∼0.5 au*

R. Bučík[1], G. M. Mason[2], N. V. Nitta[3], V. Krupar[4,5], L. Rodriguez[6], G. C. Ho[2], S. T. Hart[7,1], M. A. Dayeh[1], J. Rodríguez-Pacheco[8], R. Gómez-Herrero[8], and R. F. Wimmer-Schweingruber[9]

[1] Southwest Research Institute, 6220 Culebra Rd, San Antonio, TX 78238, USA
e-mail: radoslav.bucik@swri.org
[2] Applied Physics Laboratory, Johns Hopkins University, 11100 Johns Hopkins Rd, Laurel, MD 20723, USA
[3] Lockheed Martin Advanced Technology Center, 3251 Hanover Street, Palo Alto, CA 94304, USA
[4] Heliophysics Science Division, NASA Goddard Space Flight Center, 8800 Greenbelt Rd, Greenbelt, MD 20771, USA
[5] Goddard Planetary Heliophysics Institute, University of Maryland, Baltimore, MD 21250, USA
[6] Solar-Terrestrial Center of Excellence-SIDC, Royal Observatory of Belgium, Ringlaan -3- Av. Circulaire, 1180 Brussels, Belgium
[7] The University of Texas at San Antonio, San Antonio, TX 78249, USA
[8] Universidad de Alcalá, Space Research Group, 28805 Alcalá de Henares, Spain
[9] Institut für Experimentelle und Angewandte Physik, Christian-Albrechts-Universität zu Kiel, Leibnizstr. 11, 24118 Kiel, Germany

Received 9 January 2023 / Accepted 11 April 2023

ABSTRACT

We report Solar Orbiter observations of six recurrent solar energetic particle injections in 2022 March 3−6 at ∼0.5 au. All but one were associated with jets emanating from a plage near a large sunspot in active region 12 957. We saw large jets in injections with high ^{3}He and Fe enrichments and minor jets in injections with no or lower enrichments. Furthermore, the event with the highest enrichment showed a more compact configuration of the underlying photospheric magnetic field. The higher fluences as well as harder spectra were seen in the event with a simultaneous jet and wider eruption. However, in this case, the energy buildup time in the source might be required to produce such spectra. Extreme-ultraviolet images from Solar Orbiter revealed a number of intersecting loops at the base of jets not seen from 1 au that might be a precondition for the recurrent events.

Key words. Sun: particle emission – Sun: abundances – Sun: flares – acceleration of particles

1. Introduction

Impulsive or ^{3}He-rich solar energetic particle (SEP) events, characterized by ^{3}He and ultra-heavy ion abundances enhanced up to a factor of 10^4 above the coronal values (e.g., Mason 2007; Reames 2013), are the most unusual particle population in the Solar System. The events show high association with type III radio bursts (e.g., Nitta et al. 2006) and are accompanied by minor (B- or C-class) GOES soft X-ray flares (e.g., Nitta et al. 2006, 2015). Solar sources of ^{3}He-rich SEPs are coronal jets, but sometimes a wider eruption or just a brightening is observed (e.g., Wang et al. 2006; Nitta et al. 2015; Bučík 2020).

There are reports on ^{3}He-rich SEP events measured in clusters from subflares in single active regions (Reames et al. 1985, 1988; Mazur et al. 1996; Mason et al. 1999, 2000; Bučík et al. 2021; Ho et al. 2022) where abundance showed significant variations (Reames et al. 1988; Ho et al. 2022). Imaging observations revealed that sources of these recurrent ^{3}He-rich injections are jets from solar plages (patches of scattered magnetic fields) or coronal hole edges (Wang et al. 2006; Bučík et al. 2014; Chen et al. 2015). The works on recurrent events were from both single and angularly separated spacecraft at ∼1 au.

Driving mechanisms of repeated injections from a single source and their spectral and abundance variations on short timescales is paramount for understanding the particle acceleration in ^{3}He-rich SEP events. Measurements at close distances to the Sun, where ions would be less affected by interplanetary propagation effects, are the most appropriate to explore the variability in recurrent events. In this Letter, we report a period of recurrent ^{3}He-rich events observed by Solar Orbiter (Müller et al. 2020) at ∼0.5 au on 2022 March 3−6. We examine the activity in the solar source to understand vastly different abundances in observed ion injections. For the first time, we can explore imaging observations of a ^{3}He-rich SEP source from an unprecedented close distance to the Sun at ∼0.5 au.

2. Instrumentation

Recurrent ion events were detected by the Suprathermal Ion Spectrograph (SIS) of the Energetic Particle Detector (EPD) suite (Rodríguez-Pacheco et al. 2020) aboard Solar Orbiter. The SIS is a time-of-flight mass spectrometer that measures elemental composition from H through ultra-heavy nuclei in the kinetic

* Movies associated to Fig. 4 are available at https://www.aanda.org

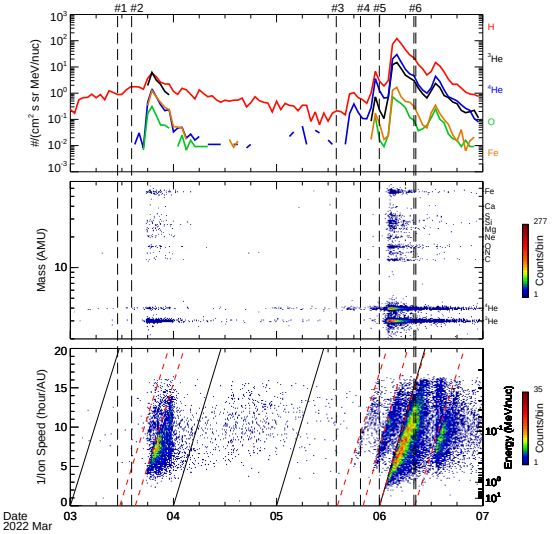

Fig. 1. Solar Orbiter SIS measurements of the recurrent events. Top: 1 h H, ^{3}He, ^{4}He, O, and Fe intensity at 0.23−0.32 MeV nucleon^{-1}. Middle: mass vs. time at 0.4−10 MeV nucleon^{-1}. Bottom: 1/(ion-speed) vs. arrival times of 10−70 AMU ions. The measurements are from both telescopes and averaged together. Sloped solid black lines mark arrival times for particles traveling along the nominal Parker interplanetary magnetic field (IMF) line without scattering. Sloped dashed red lines approximately mark ion injections. The vertical dashed lines mark type III radio bursts associated with the ion injections.

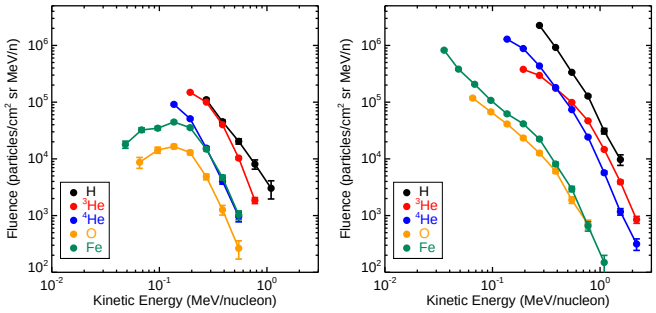

Fig. 2. Fluence spectra for selected species measured by SIS-a telescope. Left: injection #2. Right: injection #5.

energy range of ~0.1−10 MeV nucleon^{-1}. The SIS has two telescopes, one (SIS-a) pointing at 30° (sunward) and the other (SIS-b) at 160° (anti-sunward) to the west of the spacecraft-Sun line. We also used energetic ion measurements from Ultra Low Energy Isotope Spectrometer (ULEIS; Mason et al. 1998) aboard Advanced Composition Explorer (ACE), Suprathermal Ion Telescope (SIT; Mason et al. 2008) aboard Solar Terrestrial Relations Observatory A (STEREO-A), and Integrated Science Investigation of the Sun (IS⊙IS) Energetic Particle Instrument-Low Energy (EPI-Lo; Hill et al. 2017) aboard Parker Solar Probe (PSP). The solar sources of energetic particles were investigated with high-resolution observations from the Atmospheric Imaging Assembly (AIA; Lemen et al. 2012) and Helioseismic and Magnetic Imager (HMI; Scherrer et al. 2012) on the Solar Dynamics Observatory (SDO) and the Extreme-Ultraviolet Imager (EUI; Rochus et al. 2020) on Solar Orbiter. We used AIA full-disk images of the Sun with a pixel size of 0.6″ and 12 s cadence at 171 Å and 211 Å extreme-ultraviolet (EUV) bands and EUI images from the HRI_EUV (High-Resolution Instrument) with a pixel size of 0.492″ and 5 s cadence at the 174 Å EUV band (EUI Data Release 5.0 2022-04[1]). HMI has a pixel size of 0.5″ and 45 s cadence. We inspected radio spectrograms for the presence of the associated type III radio bursts. Instead of using the Solar Orbiter Radio and Plasma Waves (RPW; Maksimovic et al. 2020), which showed an enhanced level of interference at higher frequencies (>2.5 MHz), we employed data from the STEREO-A Waves instrument (Bougeret et al. 2008) that covers a frequency range of <16 MHz.

3. Energetic ion observations

Figure 1 shows the period of recurrent ion injections in 2022 March 3–6 observed by Solar Orbiter. The six injections were clearly recognized in the inverted ion-speed plot (bottom panel of Fig. 1). The injections are approximately marked by slanted dashed red lines. They were obtained using the fitting method described in Hart et al. (in prep.) for injections 2−5. This method bins pulse-height analysis data into 5-min bins and varies the energy bin sizes and centers. Each energy bin is fit to an analytical Heaviside step function multiplied by an exponential decay. The maximum of the second derivative of the resulting fit determines the onset time of the particles within the specified energy range. The energy bins are varied, and the fitted injection that minimizes chi-squared is chosen. Vertical dashed black lines mark onsets of type III radio bursts that correspond to these ion injections. Time-intensity profiles at the 0.23−0.32 MeV nucleon^{-1} (top panel of Fig. 1) and the mass spectrogram at the 0.4−10 MeV nucleon^{-1} (middle panel of Fig. 1) show no ^{3}He during injections #1 and #3, but a high amount of ^{3}He in injections #2, #5, and #6. We note that event #1 starts at an energy below the ~0.1 MeV nucleon^{-1}, and this is below the threshold for ^{3}He detection, so SIS does not show ^{3}He even if it was there earlier in the event (before Solar Orbiter connected to the source). The time-intensity profiles show a high abundance of ^{3}He relative to ^{4}He and Fe relative to O for injection #2, where very unusually the ^{3}He intensity curve lies on the H curve and Fe on ^{4}He. Furthermore, ^{3}He might even exceed H intensity that, unlike heavy ions, is enhanced before event #2. Injections #5 and #6 show similar ^{3}He abundances, which are higher than the ^{3}He abundance in injection #4. The Fe abundances are similar in injections #4 and #6, and they are smaller than the Fe abundance in injection #5 as indicated by the time-intensity profiles in Fig. 1. The highest ^{3}He and Fe relative abundances are in injection #2 (see also Table 1). Its ^{3}He- and Fe-rich enhancements are the most extreme of any event so far detected by Solar Orbiter (cf. Mason et al. 2021; Bučík et al. 2021; Ho et al. 2022).

Figure 2 shows energy spectra for the most notable injections #2 and #5. To include particles from a given injection, the energy spectra are integrated into "smoosh" boxes. For injection #2, the smoosh box is between the second slanted dashed line and March 4 00:08 UT and for injection #5 between the fifth and sixth slanted dashed lines. The O and Fe spectra in injection #2 are markedly rounded toward the low (below the ~200 keV nucleon^{-1}) energies, which is probably related to a sudden "cut" near the end of March 3 (bottom panel of Fig. 1). The O and Fe spectra in injection #5 are similar to double power laws. The ^{3}He spectra are also curved. The ^{4}He and H spectra are similar to power laws, though the ^{4}He spectrum in injection #5 is somehow rounded at low energies. Such spectra have been previously reported from 1 au measurements of ^{3}He-rich SEPs (e.g., Mason et al. 2000, 2002). There are also measurements

[1] https://doi.org/10.24414/2qfw-tr95

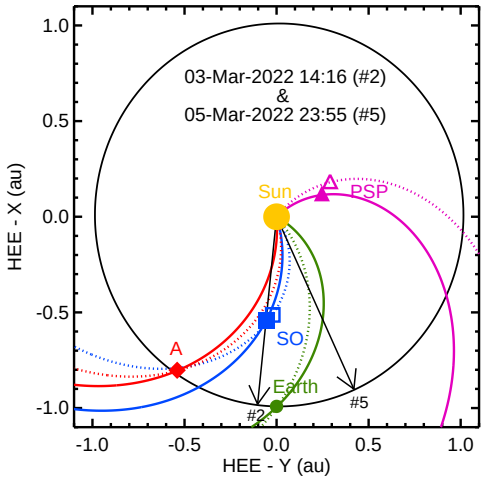

Fig. 3. Ecliptic plane projection of selected spacecraft. Filled and open squares (triangles) mark locations of Solar Orbiter (Parker Solar Probe, PSP) on 2022 March 3 at 14:16 UT and March 5 at 23:55 UT, respectively. A filled diamond and filled circle mark locations of STEREO-A (A) and the Earth on both dates, respectively. The arrows indicate the longitudes of the solar source at onsets of type III radio bursts associated with injections #2 and #5. Solid and dotted Parker IMF lines are at onsets of type III radio bursts in injections #2 and #5, respectively. The Parker IMF lines were determined from measured 1 h averaged solar wind speeds. It is important to note, however, that for injection #2, the PSP solar wind speed is not available, and the IMF line is for a nominal solar wind speed of 350 km s^{-1}.

from 1 au where spectra of all species are power laws or double power laws (e.g., Mason et al. 2000, 2002), which is not the case in these spectra. It has been discussed that similar power-law spectra for all species can be the result of the propagation of particles from the Sun to 1 au (Mason et al. 2002). To explore this further, energy spectra from other Solar Orbiter perihelia need to be obtained. We note that ^{3}He, ^{4}He, O, and Fe spectra in injection #2 fall more steeply with energy than in injection #5. Furthermore, ^{3}He fluences in injection #5 were higher than in the previous recurrent injection #2 over the measured energy range. Thus, the higher ^{3}He/^{4}He ratio in #2 compared to #5 was due to small ^{4}He fluences in injection #2. The spectra also show that ^{3}He/^{4}He increases with energy in injection #5 but remains constant over the energy range in injection #2. We note event #5 is relatively rich in Sulfur, though not as much as some rare cases reported previously (Mason et al. 2002).

Figure 3 plots the locations of selected spacecraft in the heliocentric Earth ecliptic coordinates. Solar Orbiter and STEREO-A were well connected to the source along Parker spiral interplanetary magnetic field (IMF) lines in recurrent injections #2 and #5. Near-Earth spacecraft (e.g., ACE) were well connected only to source in injection #5. PSP was not connected to the source of these injections. For clarity, the connections for other injections are not plotted. Although STEREO-A was well connected to the source during injections #2 and #5, ions were almost not detected on the spacecraft. Nominally, SIT had a sunward viewing direction close to the average Parker IMF line; however, after solar conjunction in 2015, STEREO spacecraft were rolled 180° about the spacecraft-Sun line. Consequently, the SIT field of view (FOV) is perpendicular to the Parker IMF line. Since SIS measured ~10:1 forward to backward anisotropies (not shown), the pointing of STEREO-A probably is the reason the intensities there are so low. ULEIS aboard ACE points to the sunward hemisphere at an angle of 60° to the spacecraft-Sun line. It measured the ^{3}He event during injection #5 (see Fig. A.1) when ACE was well connected to the source. We found that SIS ion fluences in injection #5 are about 20× higher than ULEIS. The Solar Orbiter distance of 0.51 au accounts only roughly for a factor of 4, implying that other effects, such as details of magnetic connection, must play a significant role. The SIS abundance ratios match the ULEIS ratios closer (see Table 1). IS⊙IS EPI-Lo PSP data show no intensity enhancement during injection #5. The data are not available for injection #2.

4. Solar source observations

Table 1 summarizes the characteristics of the recurrent injections. Type III radio bursts for injections #1 and #2 were observed by San Vito Solar Observatory (SVI) at 25−180 MHz (reported in the US National Oceanic and Atmospheric Administration (NOAA) Edited Events catalog). Type III radio bursts with an onset on March 5 at 19:32 UT (injection #4) and March 6 at 08:25 UT (injection #6) were not observed above ~1−2 MHz (see right panels in Figs. B.2 and B.3). Injection #6 is probably associated with two type III radio bursts separated by ~25 min (see Fig. B.3). The NOAA catalog lists type VI bursts on March 6 at 25−139 MHz from SVI from 08:21 to 09:04 UT. The event-associated jets and brightening occurred in the NOAA active region (AR) 12957. Injections #1, #2, and #4 show no evidence of X-ray flux enhancement; the values in Table 1 indicate levels of the background. The footpoint longitude of Solar Orbiter was obtained from a simple Parker IMF approximation using a measured solar wind speed. Employing a potential field source surface (PFSS) model, we found that the open coronal field lines (negative polarity) emanating from the AR 12957 connect to the Solar Orbiter footpoint for all injections (see also magnetic connection tool[2], Rouillard et al. 2020).

Figure 4 displays radio, soft X-ray, and EUV imaging observations of the solar source for recurrent injections #2 and #5. The figures for the remaining injections are shown in Appendix B. The running difference images in Fig. 4 (middle panels) show that injection #2 was associated with a straight long jet and injection #5 with a complex emission. The emission in injection #5 contains two simultaneous eruptions, one jet-like in the south and the other broader in the north. When approximated by ellipses, the source area of the jet in event #2 is ~280 Mm^2, and the eruption in event #5 is ~490 Mm^2. The images for injection #2 are shown at the time of 211 Å intensity maximum, and for injection #5 the images are shown three minutes after the intensity maximum when the jet-like ejection becomes clearer. Injection #1 was associated with small brightening and the remaining injections were with tiny jets. The composite images of AIA 211 Å and HMI line-of-sight magnetic field in Fig. 4 (bottom panels) and Figs. B.2 and B.3 indicate that jets in all injections originated in the plage, located westward from the two big sunspots of opposite polarities. The jets' ejection started in the region between positive (white) polarity (marked by P) and negative (black) polarity that is westward (marked by N1) of the positive polarity P. There is also negative polarity eastward (marked by N2) of the positive polarity P. Interestingly, these negative polarity areas are compact in injection #2 and more dispersed in the remaining injections. The brightening associated with injection #1 arose from a positive polarity fleck within the negative polarity site near the periphery of the negative polarity sunspot.

[2] http://connect-tool.irap.omp.eu

Table 1. Characteristics of the Solar Orbiter recurrent events.

Injection number	Heliocentric distance (au)	Type III [(a)] start (UT)	Jet [(b)] location	^{3}He/^{4}He [(c)]	Fe/O [(c)]	GOES X-ray flare	Separation [(d)] angle (°)
1	0.55	Mar.-03 11:00	E12S15 [(e)]	...	...	<B3.8	28
2	0.54	Mar.-03 14:16	E06S17	9.91±0.88	3.70±0.64	<B5.0	22
3	0.52	Mar.-05 13:54	W21S16	...	...	B6.0	1
4	0.52	Mar.-05 19:32	W24S15	0.17±0.04	...	<B7.0	1
5	0.51	Mar.-05 23:55	W26S16	0.97±0.02	1.33±0.15	C1.4	6
6	0.51	Mar.-06 07:58	W32S14 [(e)]	1.28±0.08	0.50±0.17	B7.0	5
	0.51	Mar.-06 08:25	W32S17	...	...	B6.4	4

Notes. [(a)]In STEREO-A. [(b)]In Stonyhurst heliographic system and SDO AIA 211 Å images. [(c)]Solar Orbiter SIS 0.32−0.45 MeV nucleon^{-1}. [(d)]Between the Solar Orbiter magnetic footpoint on the Sun and the jet longitude. [(e)]No jet seen only brightening. The ACE ULEIS 0.32−0.45 MeV nucleon^{-1} ^{3}He/^{4}He and Fe/O ratios for injection #5 are 1.45 ± 0.14 and 2.22 ± 0.38, respectively.

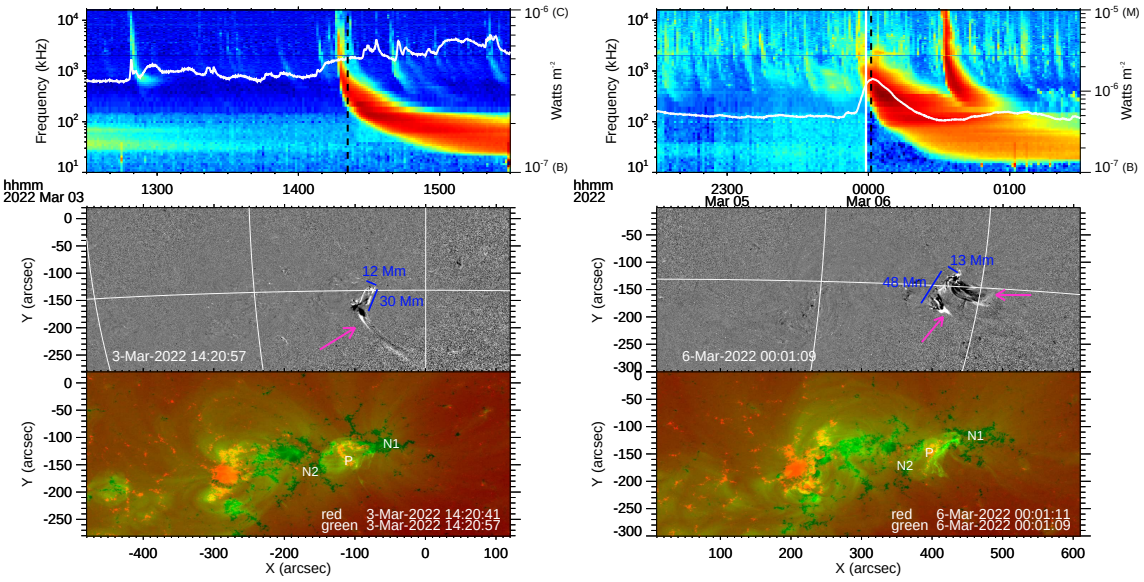

Fig. 4. Radio, soft X-ray, and EUV imaging observations of the solar source. The left (right) panels are for injection #2 (#5). Top: STEREO-A Waves radio spectrograms and GOES-16 X-ray fluxes at 1.0−8.0 Å (white curve). Color-coding in the radio spectrograms represents *E* intensity (dB > background). The right axis labels B, C, and M mark flare classes. The vertical dashed black lines mark the times of images in the middle and bottom panels. Middle: SDO AIA 211 Å 1-min running-difference images. The heliographic longitude-latitude grid has a spacing of 15°. The arrows mark a jet (left panel), as well as jet-like and wider eruptions (right panel). Line segments mark the rough estimate of the projected size of the source of the jet (right panel) and the eruption (left panel) at the time of the 211 Å intensity maximum. Bottom panels: SDO AIA 211 Å corresponds to green, and the SDO HMI line-of-sight magnetic field (scaled to ±200 G) corresponds to black and red tinted colors. Furthermore, N1 and N2 mark negative and P positive polarity patches in the ^{3}He-rich SEP source. Animations of AIA 211 Å 12 s direct images corresponding to the bottom panels are available online.

The source in event #2 shows two small bright loops and the corresponding jet spires (see images and animation in Fig. 4, left), resembling standard interchange reconnection jet (Shibata et al. 1992). In line with the reconnection model, these loops, connecting the positive-polarity area (P) and the negative-polarity area in the west (N1), would reconnect with seemingly open field lines emanating from the negative-polarity area in the east (N2). The eruptions in event #5 contain a minifilament that formed between positive polarity region P and negative polarity region N1. It is seen in the animation of Fig. 4 (right) as a dark S-shaped form on 2022 March 5 at 23:51−23:56 UT. The eruption of the minifilament as a trigger of coronal jets in active regions has been reported in previous studies (e.g., Sterling et al. 2016, 2017).

Figure 5 shows SDO AIA (top panel) and Solar Orbiter EUI HRI_EUV (bottom panel) EUV images of the area where recurrent injections originated. The high-resolution EUI HRI_EUV image is shown at the time closest to the recurrent injection #2 (~3.5 h before the injection). We lack high-resolution EUI observations at times of the injections' associated type III radio bursts. To account for light travel time (220 s) between Solar Orbiter at 0.55 au and SDO at 0.99 au, the AIA image is shown at a later time to compare with the EUI image. The Solar Orbiter image appears more structured than the SDO image which is mainly due to its closer heliocentric distance to the Sun. We note that the angular pixel size of EUI HRI_EUV and AIA are comparable (see Sect. 2). At 0.55 au, Solar Orbiter provides a factor of 2.2 better resolution than SDO. Although both the EUI 174 Å and AIA 171 Å wavelength bands observe low corona, they peak at slightly different temperatures: 174 Å near 1 MK and 171 Å near 0.8 MK. The source of ion injections is different from the neighboring region in the east where tall, closed loops connect with

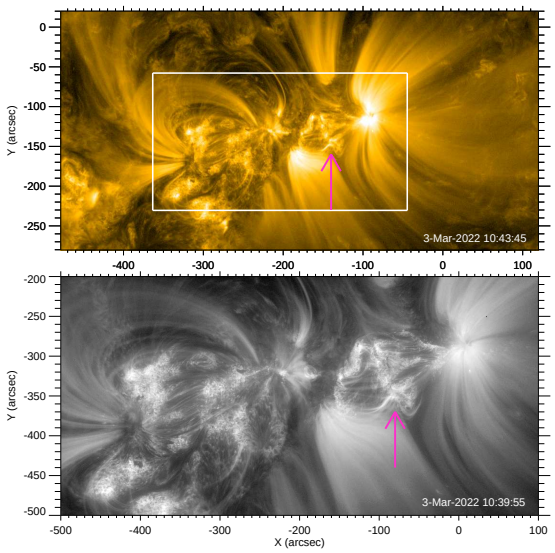

Fig. 5. Comparison of SDO and Solar Orbiter EUV images of the solar source. Top: SDO AIA 171 Å image. Bottom: Solar Orbiter EUI HRI_EUV 174 Å image at the time closest to injection #2. Solar Orbiter was at 0.55 au at that time. The arrows mark the location of the jet footpoint for injection #2. The white rectangle in the top panel indicates the bottom panel Solar Orbiter FOV.

sunspots of opposite polarities. EUI on Solar Orbiter observed a substantial number of intersecting loops in the source of ^{3}He-rich SEPs. Such a fine structure is not seen in the SDO image.

5. Summary

We examined repeated ion injections from a single source, measured by Solar Orbiter in 2022 March 3−6, when the spacecraft was at 0.51−0.55 au from the Sun. Six injections were identified within a ~3-day period.

SDO EUV imaging observations revealed a straight, large jet in the injection (#2) with the highest ^{3}He and Fe enrichments. Smaller or no ^{3}He and Fe enrichments were measured in injections (#1, #3, #4, and #6) with brightening and minor jets. The most intense injection (#5) that still shows relatively high ^{3}He enrichment was associated with the complex eruption with the source size almost twice the source of the jet in injection #2. It is consistent with the suggestion of Ho et al. (2005) that observed fluences depend on the size of the acceleration region. The energy spectrum in injection #5 was harder than the spectrum in #2. It may indicate that a time (~2.5 days in this case) is required for the magnetic energy buildup process to produce more energetic ions in the follow-up injection.

SDO HMI line-of-sight magnetograms indicated that the source of the jets in ^{3}He recurrent injections was a plage region. Injection #2, with the highest enrichments, shows compact areas of negative polarities; whereas, in other recurrent injections, the areas are more dispersed. This suggests that magnetic flux density might be related to high enrichment.

There is likely no single factor that affects the observed abundance and spectral variability in recurrent injections. We saw that these properties vary with the size and shape of the associated jets (i.e., acceleration regions) and the distribution of the photospheric field.

Solar Orbiter EUI, providing high-resolution EUV imaging observations from a closer distance (~0.55 au) to the Sun, disclosed features that were not seen from 1 au. Specifically, the ^{3}He-rich SEPs' source showed a network of crisscrossing loops that might be prone to repeated reconnection. This network may also correspond to the simulated turbulent magnetic structures arising intrinsically from magnetic reconnection in the corona (Daughton et al. 2011) that enhance particle acceleration in impulsive flares (Dahlin et al. 2015). Reames et al. (1985) suggested favorable solar escape conditions for such events. We will explore characteristics of recurrent sources further when imaging observations from Solar Orbiter perihelia capturing ^{3}He-rich jet eruptions become available.

Acknowledgements. R. Bučík was supported by NASA grants 80NSSC22K0757, 80NSSC21K1316 and NASA contract NNN06AA01C. Solar Orbiter is a mission of international cooperation between ESA and NASA, operated by ESA. The Suprathermal Ion Spectrograph (SIS) is a European facility instrument funded by ESA. The SIS instrument was constructed by the Johns Hopkins Applied Physics Lab. and CAU Kiel. Post launch operation of SIS at APL is funded by NASA contract NNN06AA01C. The UAH team acknowledges the financial support of the Spanish MINCIN Project PID2019-104863RBI00/AEI/10.13039/501100011033. The EUI instrument was built by CSL, IAS, MPS, MSSL/UCL, PMOD/WRC, ROB, LCF/IO with funding from the Belgian Federal Science Policy Office (BELSPO/PRODEX PEA C4000134088); the Centre National d'Etudes Spatiales (CNES); the UK Space Agency (UKSA); the Bundesministerium für Wirtschaft und Energie (BMWi) through the Deutsches Zentrum für Luft- und Raumfahrt (DLR); and the Swiss Space Office (SSO). We acknowledge Natalia Papitashvili at NASA/GSFC and CDAWeb for using 1 h merged magnetic field and plasma data from Solar Orbiter, STEREO-A, and near-Earth (ACE, Wind, IMP) spacecraft. Finally, we acknowledge the helpful discussions within the International Space Science Institute Team ID 425 "Origins of ^{3}He-Rich SEPs".

References

Bougeret, J. L., Goetz, K., Kaiser, M. L., et al. 2008, Space Sci. Rev., 136, 487
Bučík, R. 2020, Space Sci. Rev., 216, 24
Bučík, R., Innes, D. E., Mall, U., et al. 2014, ApJ, 786, 71
Bučík, R., Mason, G. M., Gómez-Herrero, R., et al. 2021, A&A, 656, L11
Chen, N.-H., Bučík, R., Innes, D. E., & Mason, G. M. 2015, A&A, 580, A16
Dahlin, J. T., Drake, J. F., & Swisdak, M. 2015, Phys. Plasmas, 22, 100704
Daughton, W., Roytershteyn, V., Karimabadi, H., et al. 2011, Nat. Phys., 7, 539
Hill, M. E., Mitchell, D. G., Andrews, G. B., et al. 2017, J. Geophys. Res.: Space Phys., 122, 1513
Ho, G. C., Roelof, E. C., & Mason, G. M. 2005, ApJ, 621, L141
Ho, G. C., Mason, G. M., Allen, R. C., et al. 2022, Front. Astron. Space Sci., 9, 939799
Lemen, J. R., Title, A. M., Akin, D. J., et al. 2012, Sol. Phys., 275, 17
Maksimovic, M., Bale, S. D., Chust, T., et al. 2020, A&A, 642, A12
Mason, G. M. 2007, Space Sci. Rev., 130, 231
Mason, G. M., Gold, R. E., Krimigis, S. M., et al. 1998, Space Sci. Rev., 86, 409
Mason, G. M., Mazur, J. E., & Dwyer, J. R. 1999, ApJ, 525, L133
Mason, G. M., Dwyer, J. R., & Mazur, J. E. 2000, ApJ, 545, L157
Mason, G. M., Wiedenbeck, M. E., Miller, J. A., et al. 2002, ApJ, 574, 1039
Mason, G. M., Korth, A., Walpole, P. H., et al. 2008, Space Sci. Rev., 136, 257
Mason, G. M., Ho, G. C., Allen, R. C., et al. 2021, A&A, 656, L1
Mazur, J. E., Mason, G. M., & von Rosenvinge, T. T. 1996, Geophys. Res. Lett., 23, 1219
Müller, D., St. Cyr, O. C., Zouganelis, I., et al. 2020, A&A, 642, A1
Nitta, N. V., Reames, D. V., De Rosa, M. L., et al. 2006, ApJ, 650, 438
Nitta, N. V., Mason, G. M., Wang, L., Cohen, C. M. S., & Wiedenbeck, M. E. 2015, ApJ, 806, 235
Reames, D. V. 2013, Space Sci. Rev., 175, 53
Reames, D. V., von Rosenvinge, T. T., & Lin, R. P. 1985, ApJ, 292, 716
Reames, D. V., Dennis, B. R., Stone, R. G., & Lin, R. P. 1988, ApJ, 327, 998
Rochus, P., Auchère, F., Berghmans, D., et al. 2020, A&A, 642, A8
Rodríguez-Pacheco, J., Wimmer-Schweingruber, R. F., Mason, G. M., et al. 2020, A&A, 642, A7
Rouillard, A. P., Pinto, R. F., Vourlidas, A., et al. 2020, A&A, 642, A2
Scherrer, P. H., Schou, J., Bush, R. I., et al. 2012, Sol. Phys., 275, 207
Shibata, K., Ishido, Y., Acton, L. W., et al. 1992, PASJ, 44, L173
Sterling, A. C., Moore, R. L., Falconer, D. A., et al. 2016, ApJ, 821, 100
Sterling, A. C., Moore, R. L., Falconer, D. A., Panesar, N. K., & Martinez, F. 2017, ApJ, 844, 28
Wang, Y. M., Pick, M., & Mason, G. M. 2006, ApJ, 639, 495

Appendix A: ACE ULEIS mass spectrogram during the investigated period

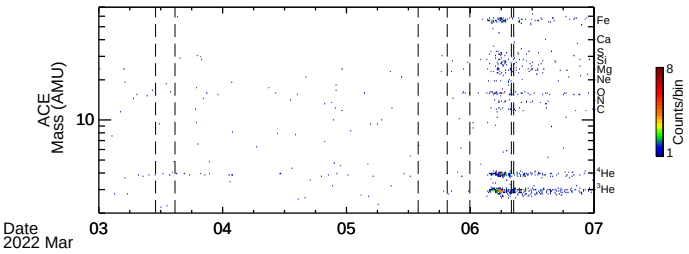

Fig. A.1. ACE ULEIS mass spectrogram at the 0.4−10 MeV nucleon^{-1}. The vertical dashed lines mark type III radio bursts associated with the recurrent ion injections detected by Solar Orbiter.

Appendix B: Radio and EUV observations for recurrent injections #1, #3, #4, and #6

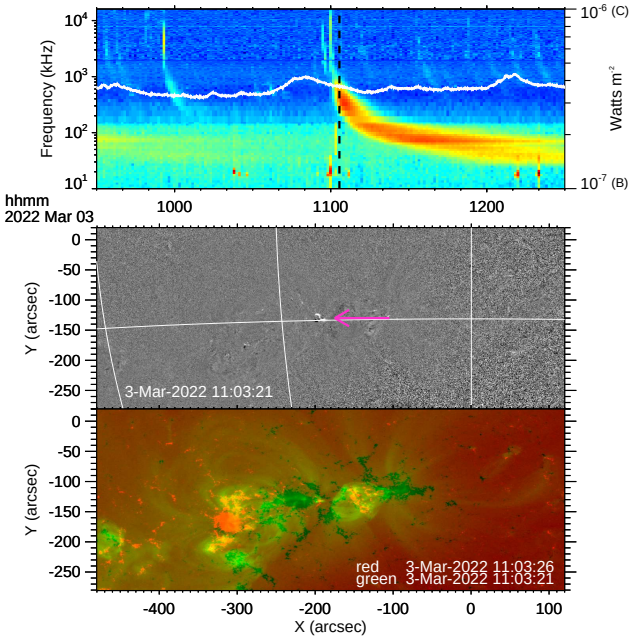

Fig. B.1. Same as Fig. 4 but for injection #1.

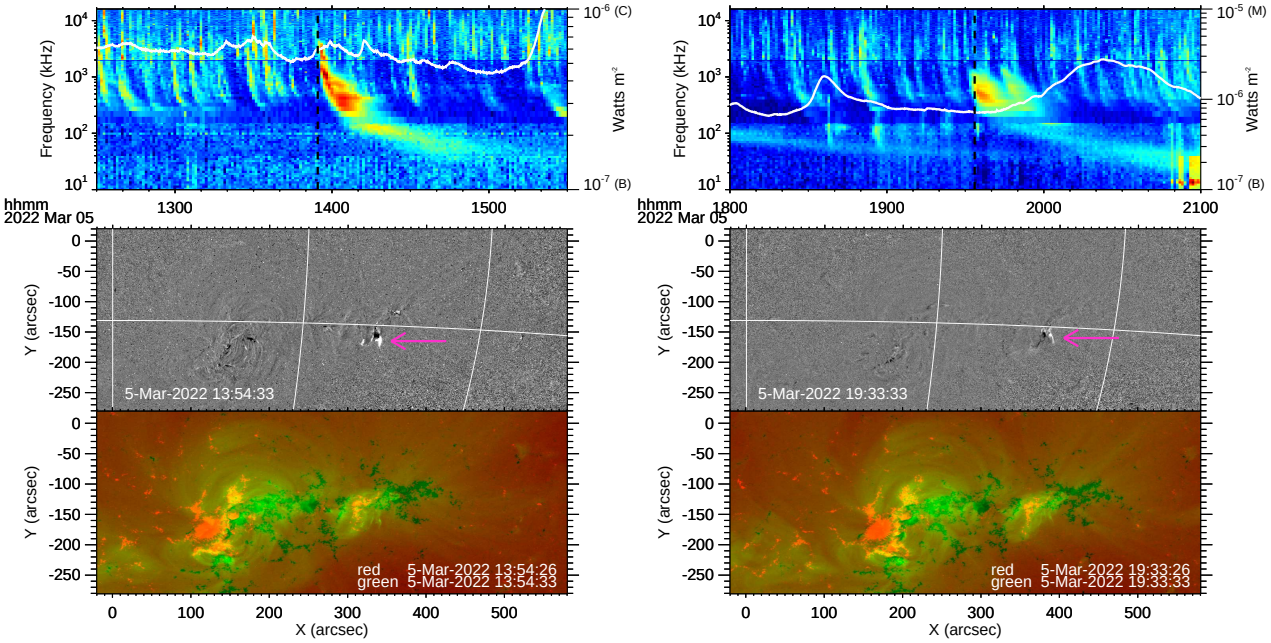

Fig. B.2. Same as Fig. 4 but for injections #3 (left panel) and #4 (right panel).

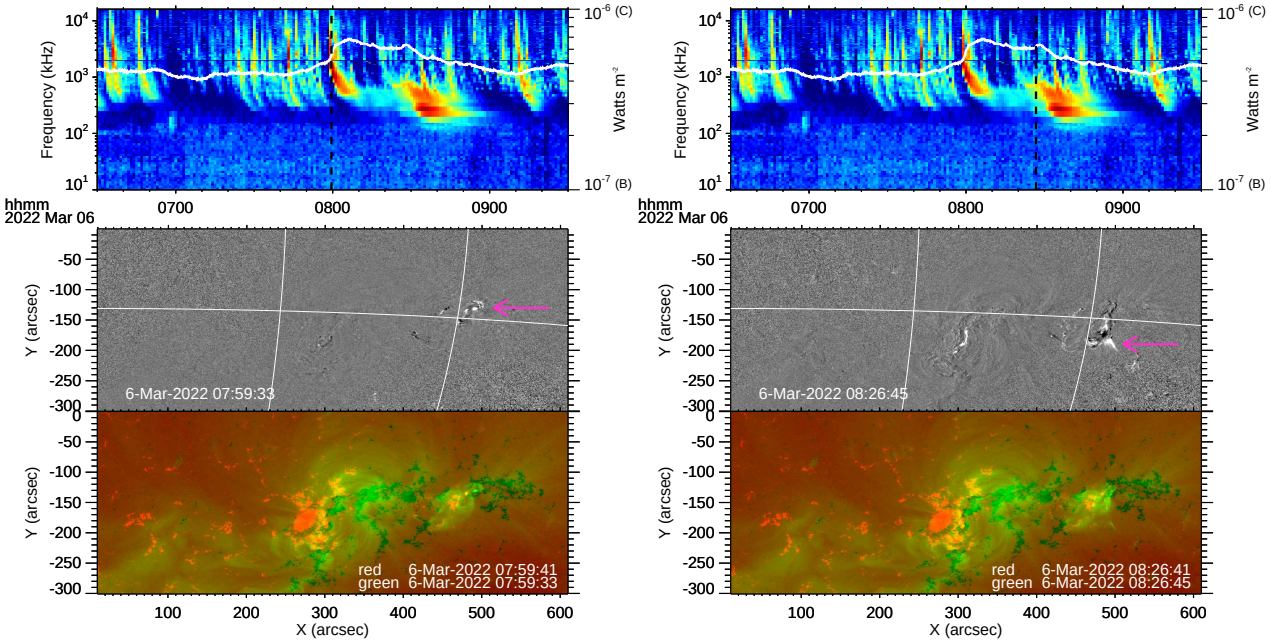

Fig. B.3. Same as Fig. 4 but for injection #6 and the first type III burst (left panel) and second type III burst (right panel).